Applied Catalysis B: Environmental 163 (2015) 123–128

Contents lists available at ScienceDirect

Applied Catalysis B: Environmental

journal homepage: www.elsevier.com/locate/apcatb

Full Length Article

Multiple exciton generation application of PbS quantum dots in ZnO@PbS/graphene oxide for enhanced photocatalytic activity

Xi-Feng Shi[a], Xin-Yuan Xia[a], Guan-Wei Cui[a,*], Ning Deng[a], Ying-Qiang Zhao[a], Lin-Hai Zhuo[b], Bo Tang[a,*]

[a] College of Chemistry, Chemical Engineering and Materials Science, Collaborative Innovation Center of Functionalized Probes for Chemical Imaging, Key Laboratory of Molecular and Nano Probes, Ministry of Education, Shandong Normal University, Jinan 250014, PR China
[b] College of Chemistry and Chemical Engineering, Taishan University, Taian 271021, PR China

ARTICLE INFO

Article history:
Received 11 May 2014
Received in revised form 24 July 2014
Accepted 25 July 2014
Available online 4 August 2014

Keywords:
Multiple exciton generation
PbS quantum dot
Graphene oxide
H_2 generation
Photocatalysis

ABSTRACT

Multiple exciton generation (MEG), also known as carrier multiplication (CM), is a process in which absorption of a single photon produces more than one electron-hole pairs. We introduce PbS QDs with multiple exciton generation (MEG) property into the construction of a novel ZnO@PbS/GO structure photocatalyst and applied to suspended photocatalytic H_2 evolution from water for the first time. The presence of multiple exciton generation process in PbS QDs, which is confirmed by transient absorption spectrum and photocurrent measurements, remarkably improves the photocatalytic efficiency of hydrogen generation combined with the electron-hole separation of GO. This strategy is proposed to open a new way for the photocatalysts design to achieve high efficiency based on QDs materials with MEG property.

1. Introduction

Multiple exciton generation (MEG), also known as carrier multiplication (CM), is a process in which absorption of a single photon produces more than one electron-hole pairs. The excess energy of an absorbed photon is used to generate extra electron-hole pairs rather than being dissipated as heat, resulting in a significant enhancement of photoelectric conversion efficiency. Since the high efficient CM in semiconductor nanocrystals (NCs) was first reported in 2004, MEG has been found in some NCs, such as PbSe [1–5], PbS [2,5,6], PbTe [7], Si [8], CdSe [9–11], InAs [12,13], InP [14] and CdTe/CdSe core–shell QDs [10].

In solar energy conversion field, the MEG effect has been successfully applied in solar cells, obtaining extraordinary photoelectron conversion efficiency [15]. An external quantum efficiency over 100% was reported by Semonin et al. on PbSe-ZnO thin film solar cell [16]. However, to the best of our knowledge, the MEG property of QDs material has not been introduced into suspended photocatalytic system because of the instability and low electron-hole separation efficiency of QDs. The aggregation of QDs would be prevented in the presence of macromolecular surfactants which, nevertheless, could cause significant hindrance of charge extraction from QDs [17,18]. Moreover, the poor electrical conductivity of QDs will discourage the charge transfer and reduce the electron-hole separation efficiency, which will aggravate the photocorrosion of QDs.

To ensure the MEG functions of QDs effectually in the photocatalytic process, both of the above-mentioned hindrances should be considered carefully, that is, the MEG QDs should disperse well in the solution without aggregation and a mass of photogenerated electrons should be exported easily from photocatalyst material. In this paper, a PbS QDs MEG photocatalytic system was elaborately constructed based on ZnO and graphene oxide (ZnO@PbS/GO) for H_2 evolution for the first time. As shown in Scheme 1, in this nanostructure, PbS QDs serve as the multiple excitons donor, ZnO serves as the carrier of PbS QDs and conduction bridge for the photoelectrons generated from PbS QDs. GO serves as the electron acceptor [19–22] and active sites provider for hydrogen production from water [23] as well as the supporting matrix to anchor nanoparticles, which can rapidly transport a mass of photoelectrons generated by MEG from PbS QDs and improve the charge separation efficiency. This assembled nanostructure can successfully prevent the aggregation of PbS QDs and overcome its poor electrical conductivity. As a result, the photocatalytic H_2 generation experiments indicated

* Corresponding authors. Fax: +86 531 8618 0017.
E-mail address: tangb@sdnu.edu.cn (B. Tang).

http://dx.doi.org/10.1016/j.apcatb.2014.07.054
0926-3373/

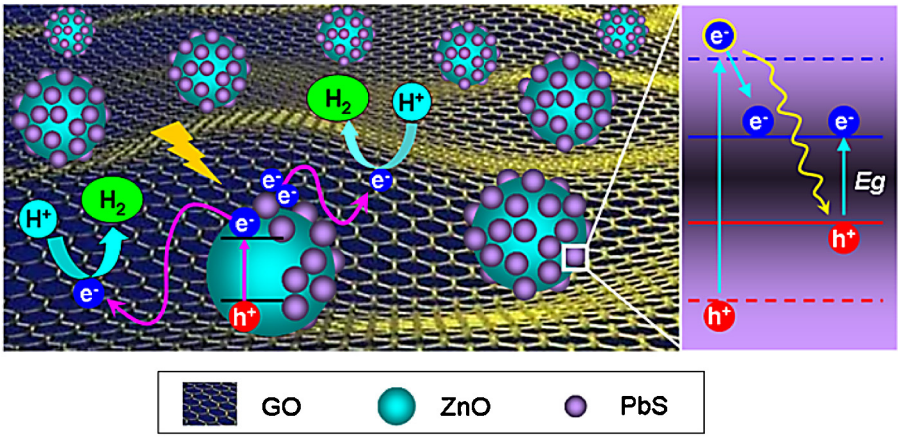

Scheme 1. Schematic illustration for the structure of ZnO@PbS/GO photocatalyst and the electron transfer mechanism.

that the MEG property of PbS QDs remarkably improves the photocatalytic efficiency combined with the electron-hole separation of GO.

2. Experimental

2.1. Materials synthesis

2.1.1. Preparation of graphene oxide (GO)

GO was prepared from purified natural graphite powder according to the improved method [24].

2.1.2. Preparation of spherical ZnO

Spherical ZnO aggregates were prepared by a solvothermal method using diethylene glycol as solvent and zinc acetate dihydrate as precursor based on a published report [25]. A more detailed synthesis process was described in the supplementary material.

2.1.3. Preparation of PbS quantum dots

Lead sulfide quantum dots (QDs) were prepared based on a published report [26]. A more detailed synthesis process was described in the supplementary material.

2.1.4. Preparation of ZnO@PbS

The loading of PbS quantum dots on ZnO was carried out by ultrasound deposition method. In a typical case, 100 mg of as-synthesized spherical ZnO, 2 mL of as-prepared PbS quantum dots dissolved in hexane (0.02 mmol mL^{-1}), and 10 mL hexane were mixed in a flask and dispersed by ultrasonic irradiation. Then, 20 mL of acetone was added into the mixture dropwise with continuous ultrasonic irradiation. The resulting product was centrifuged and dried in vacuum. Then the dried powder was calcined at 300 °C in tube furnace under Ar gas atmosphere.

2.1.5. Amination of ZnO@PbS

For the link of ZnO@PbS and GO, ZnO@PbS was modified with a bifunctional aminoethanethiol linker in which the thiol group was bound with Pb^{2+} and leaves the amino group out of PbS surfaces [27]. A more detailed synthesis process and ninhydrin experiment to detect the modification of amino was described in the supplementary material.

2.1.6. Preparation of ZnO@PbS/GO

40 mg of the as-prepared amino-modified ZnO@PbS, 20 mg of 1-hydroxybenzotriazole (HOBT) and 20 mg of 1-(3-dimethyl aminopropyl)-3-ethylcarbodiimide hydrochloride (EDC·HCl) were dispersed in 40 mL of DMF. Then 10 mL of GO solution (1 mg mL^{-1}) dissolved in DMF was added. After stirred for 24 h under room temperature, the mixture was centrifuged, washed with deionized water and dried in lyophilizer. Then the amino group modified ZnO@PbS was loaded on GO by the reaction of $-NH_2$ and —COOH, forming ZnO@PbS/GO.

2.1.7. Preparation of ZnO/GO

50 mg ZnO was dispersed in 20 mL DMF and 0.5 mL of (3-aminopropyl) triethoxysilane was added with 24 h of stirring to initiate $-NH_2$. The nanoparticles were collected by centrifugation and washed by water and ethanol. 20 mg of dried amino-modified ZnO, 10 mg of HOBT and 10 mg of EDC were dispersed in 20 mL of DMF. Then 5 mL of GO solution (1 mg mL^{-1}) dissolved in DMF was added and stirred for 24 h under room temperature to initiate ZnO/GO.

2.1.8. Preparation of PbS/GO

4 mL of as-prepared PbS quantum dots dissolved in hexane (0.02 mmol mL^{-1}), and 20 mL hexane were mixed with 10 mL GO dissolved in DMF (0.5 mg mL^{-1}) in a flask and dispersed by ultrasonic irradiation. Then 50 mL of acetone was added into the mixture dropwise with continuous ultrasonic irradiation. The resulting product was centrifuged and dried in vacuum.

2.2. Materials characterization

The methods of transmission electron microscopy (TEM), X-ray diffraction (XRD), X-ray photoelectron spectroscopy (XPS), transient absorption spectrum (TAS) measurements, and photoelectrochemical measurements were supplied in supplementary material.

2.3. Hydrogen evolution test

The photocatalytic H_2 production experiments were performed in a 20 mL Pyrex bottle at ambient temperature and atmospheric pressure, and the opening of the bottle was sealed with silicone rubber septum. Hydrogen production was performed by dispersing 20 mg of catalyst powders in a PBS buffer solution (10 mL, pH = 6.0) containing methanol (10 vol%) as sacrificial electron donor. The sample solutions were thoroughly deaerated by argon bubbling for 10 min prior to photocatalysis experiment. Each sample was irradiated by a 500 W mercury-lamp (The wavelength and relative intensity was shown in Table S1) at room temperature under constant stirring. The evolved gases were analyzed by gas chromatography (FULI 9750, TCD, Argon as the carrier gas, and 5 Å molecular sieve column). The sample was quantified by injecting

1 mL of headspace gas into the GC by a calibration plot to the external H_2 standard.

2.4. External quantum yield measurement

The hydrogen evolution test for quantum yield measurement was carried out with the same method as mentioned in hydrogen evolution test. The incident light was supplied by the nano second pulsed laser (opoltte 355 II) with the wavelength of 355 nm, of which the power passing through the samples was measured by optical power meter. The external quantum efficiency "φ" was calculated by determining the number of electrons producing the H_2 in 300 s (two electrons per H_2), which was divided by the number of incident photons in 300 s.

$$\varphi = 2n_{H2} \times 6.02 \times 10^{23}/(E \times t \times \lambda/hc)$$

E is the power of incident laser (in W), λ is taken to be 355 nm (in m), h is Planck's constant (in J/s), c is the speed of light (in m s^{-1}), n is the number of mols of generated hydrogen, t is the time (in second).

3. Results and discussion

3.1. Synthesis and characterization

The as-designed nanostructure photocatalyst was prepared by a simple multi-step assembly way. Firstly, spherical ZnO (Fig. 1a) nanoparticles with diameters of 300–500 nm were decorated with almost a single layer of PbS QDs in average size of 3–5 nm (Fig. S1) with the band gap of 1.07 eV (Fig. S2), forming ZnO@PbS (Fig. 1b). A clear lattice fringe with a crystal plane spacing of 0.298 nm (Fig. 1c) ascribed to PbS QDs showed that they were uniformly loaded on ZnO surface. The crystal structure was demonstrated by X-ray diffraction (XRD, Fig. S3) and its composition was determined by energy dispersive spectroscopy (EDS) mapping (Fig. 1d). The XRD peaks of bare ZnO and PbS QDs match well with that of hexagonal zincite (JCPDS PDF #36-1451) and cubic galena (JCPDS PDF #05-0592) respectively. The diffraction peaks of ZnO@PbS near 2θ of

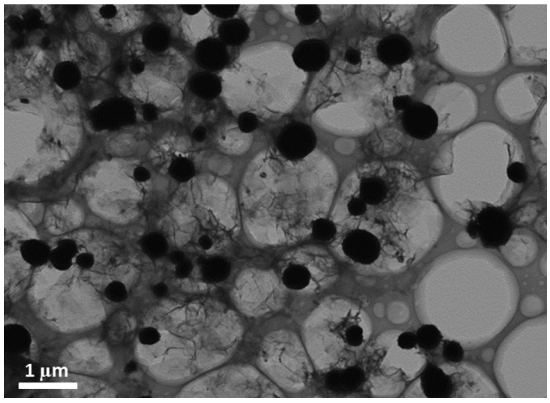

Fig. 2. TEM image of ZnO@PbS/GO complex structure.

25.9°, 30.0°, 43.1° match with PbS QDs and other peaks match well with ZnO, which indicated that PbS QDs were well crystallized on ZnO and there was no new crystal phase generated. Then the aminated ZnO@PbS (Fig. S4) by aminoethanethiol was anchored on the surface of GO by covalent amido link with good dispersity (Fig. 2). X-ray photoelectron spectroscopy (XPS, Fig. 3) was carried out to indicate the formation of amido bond, in which the peak of N1s centered at 399.9 eV is assigned to the bind energy of N atom in residual amino group in the reaction and the main peak located at 402.1 eV is attributed to the N atom in amido bond. And four peaks are observed in the C1s binding region peaks centered at 284.6 eV, 286.2 eV, 287.4 eV and 289.1 eV, which were ascribed to C*—C, C*—N, C*(O)—OH and C*(O)—NH groups, respectively.

3.2. Material photochemical properties

The MEG property of PbS QDS in the as-prepared photocatalysts was determined by femtosecond time-resolved transient absorption spectroscopy (TAS) combined with photoelectrochemical measurements. A recognized evidence of multi-exciton generation within material is the appearance of the fast multi-exciton decay

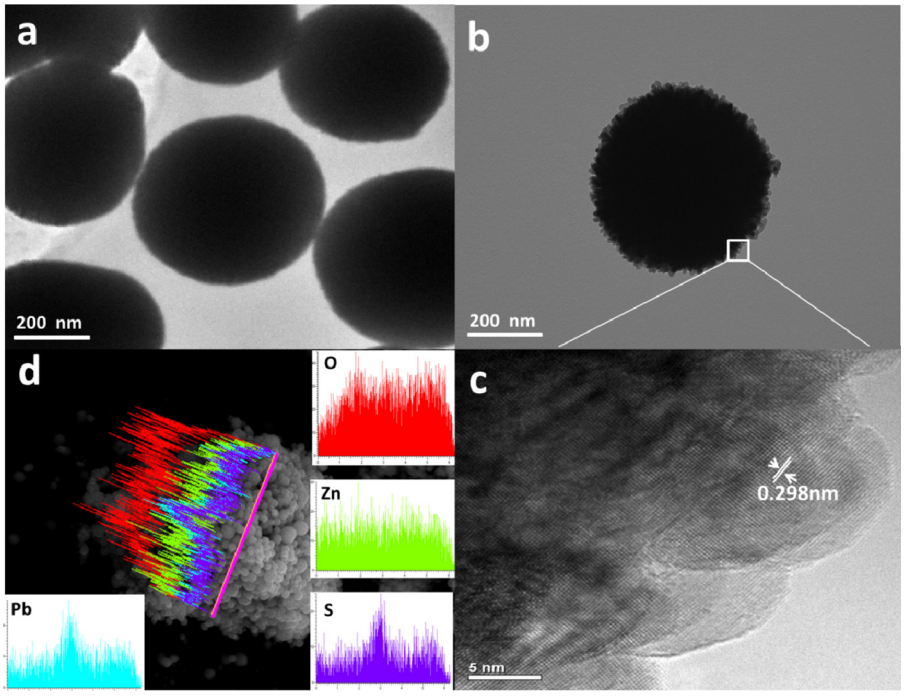

Fig. 1. (a), (b) TEM image of spherical ZnO, ZnO@PbS. (c) HRTEM of PbS QDs in ZnO@PbS. (d) EDS mapping of ZnO@PbS.

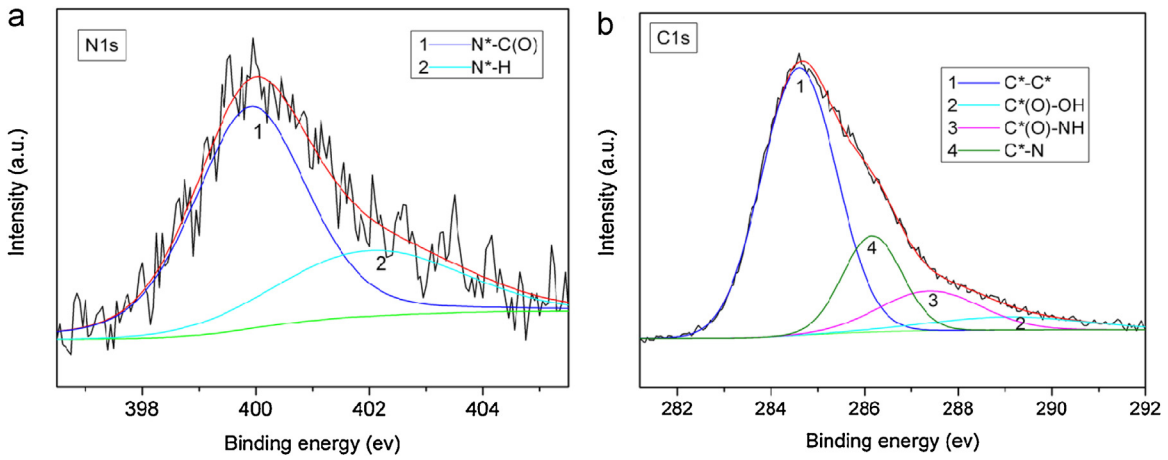

Fig. 3. High resolution X-ray photoelectron spectroscopy of N1s (a) and C1s (b) in ZnO@PbS/GO complex structure.

component when photoexciting above the energy conservation threshold (>2 Eg) at low pump fluences, for which the probability of a QD absorbing more than one photon per pump pulse is negligible [28,29]. As shown in Fig. 4a, a distinct MEG TAS feature of ZnO@PbS dispersed in hexane was observed, which was carried out pumping with 3 Eg (380 nm) photon energy and 0.1 μJ/pulse fluence. In the transient absorption spectrum, an exciton induced absorption centered at 600 nm was well consistent with the characteristic absorption region 620–600 nm of PbS QDs (Fig. 4c) [30].

The exciton kinetic traces (Fig. 4b) of ZnO@PbS exhibited a 2.2 ps short-lived decay feature followed by a 3.1 ns long-lived plateau when pumping with 3 Eg energy. It indicated that PbS QDs still have the MEG property after loading on the ZnO surface. Moreover, the short-lived exciton decay of ZnO@PbS was much faster than the 8.0 ps (Fig. 4d) of PbS QDs, which indicated that the introduction of ZnO contributed to the transfer of electrons generated from MEG of PbS QDs. However, for the ZnO@PbS/GO material, it is difficult to obtain an MEG TAS of PbS QDs because the required

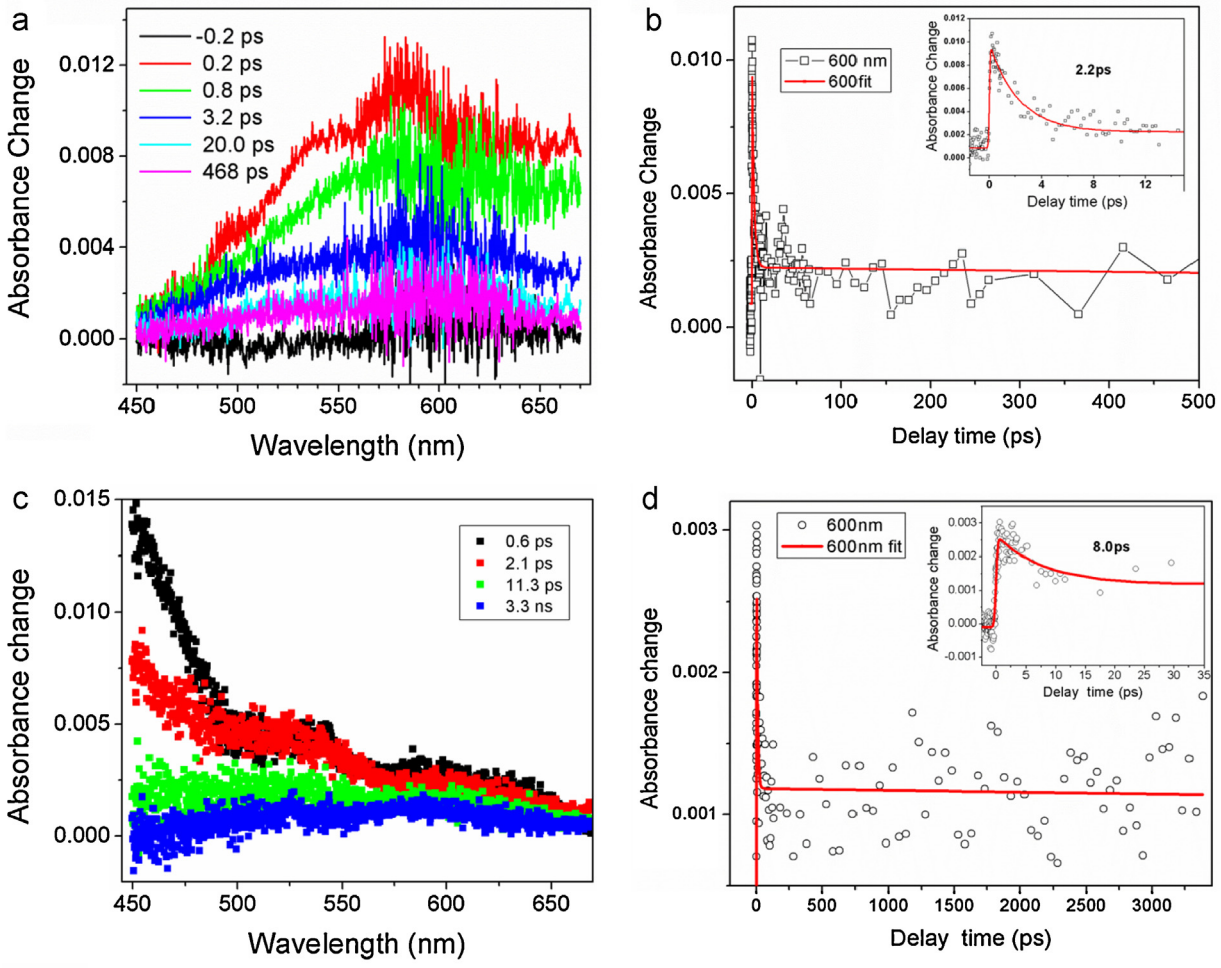

Fig. 4. Transient absorption spectrum and kinetic trace of excitons decay for ZnO@PbS (a, b) and PbS QDs (c, d) in hexane.

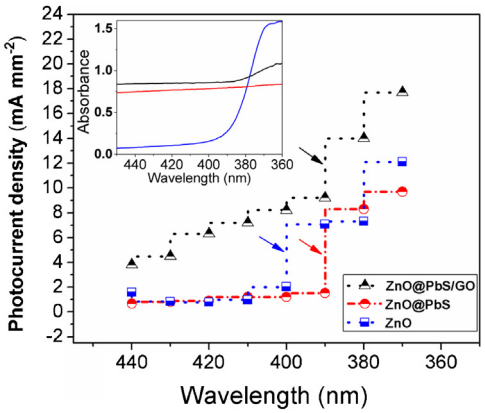

Fig. 5. Changes of photocurrent density for ZnO, ZnO@PbS and ZnO@PbS/GO irradiated under different photon energy (Inset: absorption spectrum of ZnO, ZnO@PbS and ZnO@PbS/GO in UV region).

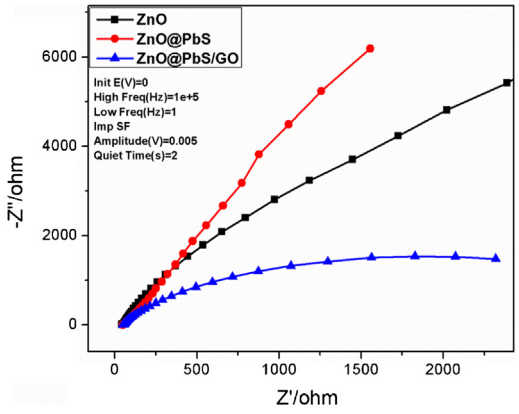

Fig. 6. Electrochemical impedance spectroscopy (EIS) Nynquist plots of ZnO, ZnO@PbS, ZnO@PbS/GO electrodes in dark.

weak test light will be absorbed by GO which has high light absorbing ability. Therefore, to further confirm the MEG property of PbS QDs in ZnO@PbS/GO, the transient photocurrent for photocatalysts was investigated under femtosecond pulse laser radiation with different wavelength at constant photo intensity. The bias voltage of 0.5 V was selected by the I–V test of ZnO@PbS/GO (Fig. S5), at which there was no photo redox reaction. As shown in Fig. 5, for ZnO@PbS and ZnO@PbS/GO materials, the photocurrent density increased gradually with the increase of irradiation energy from 2.82 eV (440 nm) to 3.18 eV (390 nm) ascribed to the enhanced electron kinetic energy and thermal energy. With the continuous increase of incident photon energy beyond up to 3.18 eV, although the light absorbance intensity was still smooth (Fig. 5, inset), an abrupt increase of transient photocurrent density was observed at 3.26 eV of photon energy (380 nm), which was 3 Eg of PbS QDs. Moreover, the photocurrent density of ZnO@PbS/GO has the same variation tendency and higher absolute value compared with that of ZnO@PbS. The abrupt increase of transient photocurrent density was owned to multiple electrons generated by the MEG process of PbS QDs. As comparison, for bare ZnO material, there was also an abrupt increase of transient photocurrent density, but it was from 400 nm of irradiation wavelength, which was different from the 380 nm for ZnO@PbS and ZnO@PbS/GO. It was well known that there was no MEG process in ZnO material and the abrupt photocurrent increase of ZnO was well consistent with the abrupt absorption of ZnO from 400 nm to 370 nm. Moreover, the abrupt photocurrent increase of ZnO from 400 nm to 390 nm was about 3.5 times and that of PbS QDs decorated ZnO from 390 nm to 380 nm was 5.4 times, which indicated that the light absorption contribution of ZnO for the photocurrent abrupt was very limited. Therefore, it can be concluded that the significant photocurrent increase of ZnO@PbS and ZnO@PbS/GO was resulted from the exciton multiplication of PbS QDs rather than the absorption enhancement of ZnO. The results suggested that the MEG property of PbS QDs still existed after introduced to the complex photocatalyst and was not negatively affected by the existence of ZnO and GO.

Whether the large number of photoelectrons generated by MEG progress could be exported easily from the material is one of the key factors for the application of MEG PbS QDs, which was evaluated here by photocurrent density under Hg lamp irradiation. The electrochemical impedance test showed that the diameter of arc radius on the EIS Nynquist plot of ZnO@PbS/GO electrode was smaller than that of ZnO electrode and ZnO@PbS electrode (Fig. 6). The smaller the arc radius of an EIS Nynquist plot demonstrated the higher the efficiency of charge separation, which indicated that the photo induced electrons and holes were easily separated for the introduction of GO [31]. The photocurrent density at the bias voltage of 0.5 V as mentioned above for each photocatalyst irradiated by Hg lamp was shown in Fig. S9. Although, as mentioned above, PbS QDs still have apparent MEG property after loading on ZnO, a lower photocurrent of ZnO@PbS even than that of bare ZnO was observed, which indicated that the photogenerated electrons were hard to be exported due to the poor electrical conductivity of PbS QDs. However, when ZnO@PbS was hybridized with GO which has good electronic conductivity, the as-prepared ZnO@PbS/GO showed the highest photocurrent density, showing that GO plays an important role in the high output of the photoelectrons generated by MEG process of PbS QDs.

3.3. Photocatalytic properties

The photocatalytic H_2 generation was employed to investigate the contribution of MEG PbS QDs for the photocatalytic activity of the as-prepared ZnO@PbS/GO. For comparison, ZnO/GO was synthesized by the same covalent link method as ZnO@PbS/GO. PbS/GO was prepared by ultrasonic deposition and the amount of PbS QDs was nearly equal to that of ZnO@PbS. As shown in Fig. 7, when ZnO was hybridized with GO, the amount of H_2 evolution was distinctly improved to 22.96 $\mu mol\, g^{-1}\, h^{-1}$ compared with that of bare ZnO (13.78 $\mu mol\, g^{-1}\, h^{-1}$) due to the excellent electrons conductivity of GO. For the ZnO@PbS/GO, the photoactivity was further improved to 34.48 $\mu mol\, g^{-1}\, h^{-1}$, higher than that of ZnO/GO (22.96 $\mu mol\, g^{-1}\, h^{-1}$) and PbS/GO (16.08 $\mu mol\, g^{-1}\, h^{-1}$), which was owned to the MEG contribution of PbS QDs and uniform dispersity of ZnO@PbS on GO to gain a good electron conduction. However,

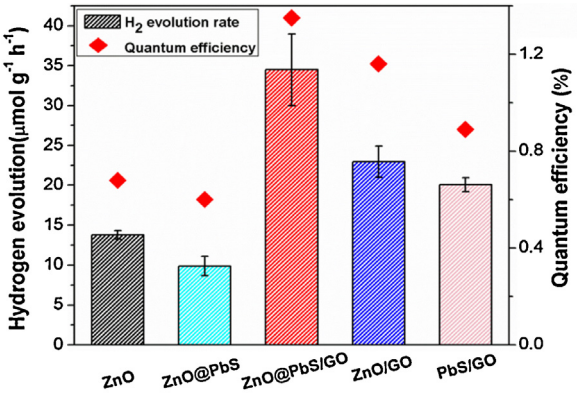

Fig. 7. Hydrogen evolution rate and quantum efficiency catalysed by ZnO, ZnO@PbS, ZnO@PbS/GO, ZnO/GO and PbS/GO in pH = 6.0 PBS buffer solution.

for ZnO@PbS, although there was apparent MEG property of PbS QDs, it showed a lower photoactivity of 9.87 $\mu mol\, g^{-1}\, h^{-1}$ even than that of bare ZnO, which was ascribed to the inner recombination of photogenerated carriers resulted from the poor electrical conductivity of PbS QDs. The external quantum efficiency of each sample was also measured which was well consistent with the hydrogen evolution activity. It demonstrated that the MEG effect of PbS QDs cooperated with electrons conductivity of GO could significantly improve the photocatalytic activity of the as-constructed ZnO@PbS/GO.

3.4. Photostability of PbS QDs in ZnO@PbS/GO

The photocatalytic activity of QDs photocatalysts will decrease after continuous light irradiation which is presumably due to the photo-oxidation of narrow bandgap semiconductors, a well-known phenomenon especially in the presence of H_2O[32–34]. For the ZnO@PbS/GO photocatalyst, the H_2 evolution efficiency was decreased after three cycles (8 h continuous UV light irradiation every cycle). X-ray photoelectron spectrum (XPS) was employed to probe the oxidation state change in PbS QDs before and after photocatalytic reaction. As shown in Fig. S10, according to the bonding energy peak area contents, approximately 14% of PbS QDs in ZnO@PbS/GO was oxidized to Pb-O adducts in the form of PbO or $PbSO_4$. It indicated that the introduction of GO and sacrificial reagent in the photocatalytic system, could suppress the photo-oxidation of PbS QDs effectively compared with that reported before [35].

4. Conclusions

We constructed a novel ZnO@PbS/GO photocatalyst by the introduction of PbS QDs with multiple exciton generation (MEG) property and applied in suspended photocatalytic system for hydrogen evolution from water. The MEG property of PbS QDs in the as-prepared ZnO@PbS/GO was well confirmed by transient absorption spectrum and transient photocurrent measurements irradiated by femtosecond pulse laser. It demonstrated that the MEG process of PbS QDs in the ternary structure combined with GO material could remarkably enhance the photoactivity of H_2 evolution reaction. The established strategy is proposed to be favorable for photocatalysts design by introducing MEG property materials to achieve high efficiency in photocatalysis research field.

Acknowledgements

This work was supported by 973 Program (2013CB933800), National Natural Science Foundation of China (21227005, 21390411, 91313302, 21035003, 21301110) and Program for Changjiang Scholars and Innovative Research Team in University.

Appendix A. Supplementary data

Supplementary data associated with this article can be found, in the online version, at http://dx.doi.org/10.1016/j.apcatb.2014.07.054.

References

[1] R.D. Schaller, V.I. Klimov, Phys. Rev. Lett. 92 (2004), 186601/1-4.
[2] R.J. Ellingson, M.C. Beard, J.C. Johnson, P. Yu, O.I. Micic, A.J. Nozik, A. Shabaev, A.L. Efros, Nano Lett. 5 (2005) 865–871.
[3] M.T. Trinh, A.J. Houtepen, J.M. Schins, T. Hanrath, J. Piris, W. Knulst, A.P.L.M. Goossens, L.D.A. Siebbeles, Nano Lett. 8 (2008) 1713–1718.
[4] M. Ji, S. Park, S.T. Connor, T. Mokari, Y. Cui, K.J. Gaffney, Nano Lett. 9 (2009) 1217–1222.
[5] G. Nair, S.M. Geyer, L.-Y. Chang, M.G. Bawendi, Phys. Rev. B 78 (2008), 125325/1-10.
[6] R.D. Schaller, M. Sykora, J.M. Pietryga, V.I. Klimov, Nano Lett. 6 (2006) 424–429.
[7] J.E. Murphy, M.C. Beard, A.G. Norman, S.P. Ahrenkiel, J.C. Johnson, P. Yu, O.I. Micic, R.J. Ellingson, A.J. Nozik, J. Am. Chem. Soc. 128 (2006) 3241–3247.
[8] M.C. Beard, K.P. Knutsen, P. Yu, J.M. Luther, Q. Song, W.K. Metzger, R.J. Ellingson, A.J. Nozik, Nano Lett. 7 (2007) 2506–2512.
[9] R.D. Schaller, M. Sykora, S. Jeong, V.I. Klimov, J. Phys. Chem. B 110 (2006) 25332–25338.
[10] D. Gachet, A. Avidan, I. Pinkas, D. Oron, Nano Lett. 10 (2010) 164–170.
[11] R.D. Schaller, M.A. Petruska, V.I. Klimov, Appl. Phys. Lett. 87 (2005), 253102/1-3.
[12] R.D. Schaller, J.M. Pietryga, V.I. Klimov, Nano Lett. 7 (2007) 3469–3476.
[13] J.J.H. Pijpers, E. Hendry, M.T.W. Milder, R. Fanciulli, J. Savolainen, J.L. Herek, D. Vanmaekelbergh, S. Ruhman, D. Mocatta, D. Oron, A. Aharoni, U. Banin, M. Bonn, J. Phys. Chem. C 111 (2007) 4146–4152.
[14] S.K. Stubbs, S.J.O. Hardman, D.M. Graham, B.F. Spencer, W.R. Flavell, P. Glarvey, O. Masala, N.L. Pickett, D.J. Binks, Phys. Rev. B 81 (2010), 081303/1-4.
[15] J.B. Sambur, T. Novet, B.A. Parkinson, Science 330 (2010) 63–66.
[16] O.E. Semonin, J.M. Luther, S. Choi, H.Y. Chen, J. Gao, A.J. Nozik, M.C. Beard, Science 334 (2011) 1530–1533.
[17] A.P. Alivisatos, J. Phys. Chem. 100 (1996) 13226–13239.
[18] H. Zhu, T. Lian, Energ. Environ. Sci. 5 (2012) 9406–9418.
[19] P. Wang, J. Xian, J. Chen, Y. He, J. Wang, W. Li, Y. Shao, D. Li, Appl. Catal. B: Environ. 144 (2014) 644–653.
[20] C. Nethravathi, T. Nisha, N. Ravishankar, C. Shivakumara, M. Rajamathi, Carbon 47 (2009) 2054–2059.
[21] P. Wang, T. Jiang, C. Zhu, Y. Zhai, D. Wang, S. Dong, Nano Res. 3 (2010) 794–799.
[22] L. Shen, M. Zeng, S.-W. Yang, C. Zhang, X. Wang, Y. Feng, J. Am. Chem. Soc. 132 (2010) 11481–11486.
[23] Y.K. Kim, H. Park, Appl. Catal. B: Environ. 125 (2012) 530–537.
[24] D.C. Marcano, D.V. Kosynkin, J.M. Berlin, A. Sinitskii, Z. Sun, A. Slesarev, L.B. Alemany, W. Lu, J.M. Tour, ACS Nano 4 (2010) 4806–4814.
[25] D. Wu, Z. Gao, F. Xu, J. Chang, W. Tao, J. He, S. Gao, K. Jiang, CrystEngComm 15 (2013) 1210–1217.
[26] M.A. Hines, G.D. Scholes, Adv. Mater. 15 (2003) 1844–1849.
[27] C. Ratanatawanate, C. Xiong, K.J.Jr. Balkus, ACS Nano 2 (2008) 1682–1688.
[28] D.J. Binks, Phys. Chem. Chem. Phys. 13 (2011) 12693–12704.
[29] M.C. Beard, J. Phys. Chem. Lett. 2 (2011) 1282–1288.
[30] Y. Yang, W. Rodriguez-Cordoba, T. Lian, Nano Lett. 12 (2012) 4235–4241.
[31] L.-W. Zhang, H.-B. Fu, Y.-F. Zhu, Adv. Funct. Mater. 18 (2008) 2180–2189.
[32] L. Spanhel, M. Haase, H. Weller, A. Henglein, J. Am. Chem. Soc. 109 (1987) 5649–5655.
[33] X. Wang, L. Qu, J. Zhang, X. Peng, M. Xiao, Nano Lett. 3 (2003) 1103–1106.
[34] X. Hu, X. Gao, ACS Nano 4 (2010) 6080–6086.
[35] C. Wang, R.L. Thompson, P. Ohodnicki, J. Baltrus, C. Matrang, J. Mater. Chem. 21 (2011) 13452–13457.